ChemElectroChem

Research Article
doi.org/10.1002/celc.202101366

Chemistry Europe
European Chemical Societies Publishing

www.chemelectrochem.org

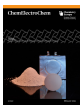

The Impact of Lithium Tungstate on the Densification and Conductivity of Phosphate Lithium-Ion Conductors

Philipp Odenwald,*[a, b] Qianli Ma,[a] Bambar Davaasuren,[a, c] Enkhtsetseg Dashjav,[a] Frank Tietz,[a, d] Michael Wolff,[a] Wolfgang Rheinheimer,[a] Sven Uhlenbruck,[a, d] Olivier Guillon,[a, d, e] and Dina Fattakhova-Rohlfing*[a, b, d]

Phosphate lithium-ion conductors are outstanding electrolyte materials for solid-state lithium batteries. As polycrystalline ceramics, they must be sintered at high temperatures. Lithium tungstate Li_2WO_4 (LWO) is reported for the first time as an effective sintering aid to reduce the sintering temperature for one of the most common solid-state lithium-ion conductors, $Li_{1.5}Al_{0.5}Ti_{1.5}(PO_4)_3$ (LATP). While densification of LATP without sintering aids requires temperatures of at least 950 °C to obtain a relative density of 90 %, here relative densities of 90–95 % are achieved even at 775 °C when 5 wt.% of LWO are added. At 800 °C the LATP containing 5–7 wt.% LWO densifies to a relative density of 97.2 %. The ionic conductivity of LWO containing LATP is generally higher than that of pure LATP sintered at the same temperature. LATP containing 7 wt.% LWO shows high ionic conductivity of 4.4×10^{-4} S/cm after sintering at 825 °C. A significant reduction in sintering temperature, an increase in density and in the ionic conductivity of LATP as well as its non-toxicity render LWO a very promising sintering aid for the development of LATP-based solid state batteries.

Introduction

Solid-state lithium ion conductors are intensively investigated as electrolytes for the next generation of lithium ion batteries (LIB), as they hold a promise to improve energy density, mechanical stability and safety of LIBs.[1] Among different classes of solid ionic conductors such as sulfide, polymer and halogenide electrolytes, ceramic oxide and phosphate electrolytes attract attention due to their reasonably high conductivity at room temperature, chemical and electrochemical stability, scalable synthesis, and simple processing.[2] The most investigated solid-state ceramic Li^+ electrolytes are the garnet $Li_7La_3Zr_2O_{12}$ (LLZO) and the NaSICON type systems with the general formula $Li_{1+x}Al_xTi_{2-x}(PO_4)_3$ ($0<x<0.5$) (LATP).[1a,2a] The LATP system offers many advantages such as high ionic conductivity (10^{-4}–10^{-3} S/cm), high oxidation stability, mechanical strength and low density and thus high specific energy of the battery cells.[3] Moreover, LATP consists of abundant and inexpensive constituents and can be produced on a large scale.[2b] The combination of these properties makes LATP electrolytes technologically and economically attractive, with some LATP-based solid state battery concepts already being commercialized.[4]

In spite of progress achieved in the last years, there are still persisting challenges that limit the use of LATP in batteries. Effective ion conduction as well as mechanical strength can only be achieved when the powder particles are well-sintered to a high-density microstructure. The consolidation and densification of LATP generally requires elevated temperatures of >900 °C.[2b] However, due to an anisotropy in thermal expansion coefficient, the densification and grain growth at high temperatures and subsequent cooling can result in mechanical stresses and even cracks which decrease the total ionic conductivity.[5] High sintering temperatures can also lead to severe chemical reactions with active materials on the cathode side, which may result in a complete failure of the battery cell and should be avoided.[6] Due to these reasons, the lowering of the processing temperature and the reduction of sintering time are desirable for the mitigation of processing-induced reactions at the interfaces between the cathode and the solid electrolyte.[7]

[a] P. Odenwald, Dr. Q. Ma, Dr. B. Davaasuren, Dr. E. Dashjav, Dr. F. Tietz, Dr. M. Wolff, Dr. W. Rheinheimer, Dr. S. Uhlenbruck, Prof. Dr. O. Guillon, Prof. Dr. D. Fattakhova-Rohlfing
Institute of Energy and Climate Research – Materials Synthesis and Processing (IEK-1)
Forschungszentrum Jülich GmbH
52425 Jülich, Germany
E-mail: p.odenwald@fz-juelich.de
d.fattakhova@fz-juelich.de
[b] P. Odenwald, Prof. Dr. D. Fattakhova-Rohlfing
Faculty of Engineering and Center for Nanointegration Duisburg-Essen (CENIDE)
Universität Duisburg-Essen
Lotharstraße 1, 47057
Duisburg, Germany
[c] Dr. B. Davaasuren
Core Labs
King Abdullah University of Science and Technology (KAUST)
23955-6900 Thuwal, Saudi Arabia
[d] Dr. F. Tietz, Dr. S. Uhlenbruck, Prof. Dr. O. Guillon, Prof. Dr. D. Fattakhova-Rohlfing
Helmholtz Institute Münster,
Ionics in Energy Storage (IEK-12)
Forschungszentrum Jülich GmbH
52425 Jülich, Germany
[e] Prof. Dr. O. Guillon
Jülich-Aachen Research Alliance,
JARA-Energy
52425 Jülich, Germany

One of the most common approaches to decrease the densification temperature of polycrystalline materials is the use of sintering aids that wet the interfaces between the primary particles and lead to densification at lower temperatures (so called transient liquid phase sintering).[8] Numerous compounds including $Li_2B_4O_7$,[2b] Li_3PO_4,[9] Li_3BO_3,[9] $LiBO_2$,[10] LiF,[11] Li_2CO_3,[9b] $LiBF_4$[12] and Bi_2O_3[13] have been studied as sintering aids for the densification of LATP and it was demonstrated that a reduction of the sintering temperature to 800 °C can be achieved. Still, our knowledge on possible sintering aids is incomplete and needs to be improved for high-performance LATP-based solid state battery concepts. Our motivation is to avoid the disadvantages connected to high sintering temperatures, by lowering the temperature. The approach chosen here used Li_2WO_4 as sintering aid.

Lithium tungstate (Li_2WO_4), a material with a low melting temperature of 742 °C,[14] was investigated in this study as a sintering aid for a LATP electrolyte for the first time. A detailed analysis of the densification behavior, evolution of the microstructure and impact on the conductivity demonstrates that lithium tungstate significantly reduces the sintering temperature and yields a very high ionic conductivity.

Results and Discussion

To ensure the compatibility of the obtained results, all experiments described in this work were obtained using the same batch (500 g) LATP, which was synthesized by SASSR (see Experimental part for the synthesis details). The elemental composition according to inductively coupled plasma optical emission spectroscopy (ICP-OES) matched well to the nominal composition (Table 1).

According to Rietveld refinements presented later in Figure 4, the reaction product corresponds mainly to a rhombohedral LATP phase containing 5% of Li_4TiPO_5 and even less $Al(PO_4)$ as impurities.

To investigate the influence of LWO on the sintering behavior of LATP, the calcined powder was ground in a planetary ball mill. The LATP powders after ball milling have a mean particle size of 0.21 μm with a bimodal particle size distribution with the presence of small particles between 0.1 μm and 0.5 μm as well as larger agglomerates with sizes between 1.1 μm and 8 μm, which was determined by Laser diffraction (Figure 1a).

The pellets were sintered at temperatures ranging from 750 °C to 900 °C for 4.5 h. The strong effect of LWO on the densification of LATP can already be deduced from the optical appearance of the pellets. The diameters visibly decrease with the increasing amount of LWO up to 7 wt.% (Figure 1b).

Dilatometry analysis recording the shrinkage curves of pressed pellets is presented in Figure 2. For all pellet compositions, no shrinkage occurs up to 650 °C. Shrinkage at the beginning of the measurement is attributed to mechanical setting effects of the measurement cell, while the elongation up to about 600 °C relates to the thermal expansion. For the

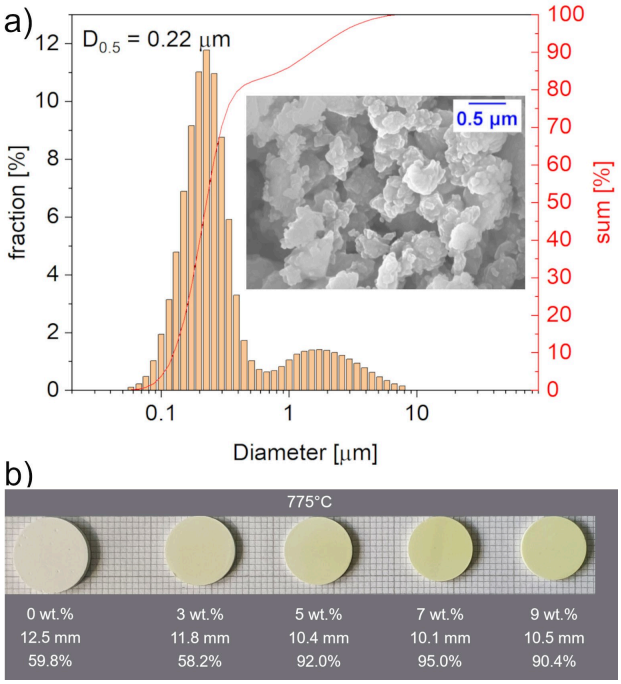

Figure 1. (a) Particle size distribution of LATP powder after ball milling. The inset shows a SEM image of the milled particles. (b) Photographs of LATP pellets containing different amount of Li_2WO_4 (LWO) after sintering at 775 °C for 4.5 hours.

Table 1. ICP-OES analysis of LATP sintered at 900 °C and crushed (normalized to 3 mol phosphorus per formula unit).

Element[1]	Atomic ratio	Nominal Composition	Deviation [%]
Li	1.42	1.5	5.3
Al	0.47	0.5	6.0
Ti	1.57	1.5	4.7
P	3.00	3.0	

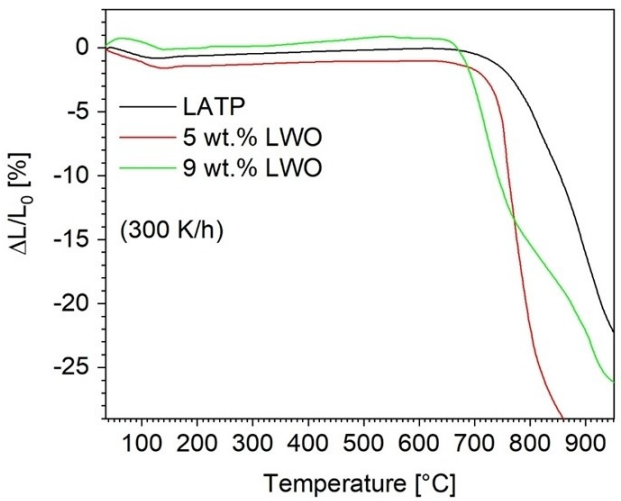

Figure 2. Shrinkage curves for a heating rate of 300 K/h for three additive concentrations (relative densities: LATP – 86.2%, 5 wt.% – 81.0%, 9 wt.% – 73.8%).

pure LATP (0 wt.% LWO), the onset of sintering is observed at about 760 °C and the densification plateau is reached at 985 °C. The onset of sintering shifts to lower temperatures with increasing LWO content to 700 °C and 672 °C (first shoulder) for the pellets containing 5 wt.% and 9 wt.%, respectively. For the pellet with 0 wt.% LWO, the linear shrinkage by sintering reaches 25% at 985 °C. For 5 wt.% LWO, the linear shrinkage reaches 31% at 880 °C, after which the shrinkage rate decreases. A second shoulder is observed at around 800 °C associated most likely with the melting of LWO at 742 °C. For 9 wt.% LWO, the densification curve shows two shoulders as well. The first part of shrinkage occurs between 672 °C and about 750 °C, followed by a second one between 750 °C and 940 °C, where a linear shrinkage of about 26% is reached.

In general, the occurrence of two shoulders in a densification curve implies the existence of two different sintering mechanisms.[8] As LWO melts at 742 °C,[15] the second shoulder from 750 °C for 9 wt.% LWO is very likely attributed to liquid phase sintering as detailed later. As the dilatometry is performed with a heating rate of 300 K/h up to temperatures of 1100 °C and no holding time only low relative densities were achieved. It shows the temperatures at which shrinking behavior is changing. The relative densities cannot be compared with the results from the sintering studies (Figure 3) with a holding time of 4.5 h at an elevated temperature.

The strong impact of the LWO on the sintering behavior of LATP also becomes obvious in the relative density after sintering for 4.5 h (Figure 3). Pure LATP shows only little densification below 950 °C. Sintering does not start before 825 °C and the density reaches only 70% at 900 °C. Significant densification of pure LATP requires temperature of 950 °C, but still does not reach more than 90%. In contrast, the addition of 3 wt.% LWO results in significant densification (80%) already at 800 °C and 90% at 825 °C. For LWO concentrations of 5 wt.% or higher, relative densities of around 80–85% are obtained already at 750 °C, and densities of 90–95% are achieved at 775 °C. This again agrees well with the melting temperature of LWO at 742 °C. At a temperature of 800 °C the LATP containing 5–7 wt.% LWO densifies nearly completely to a relative density of 97.2%, which increases even further to 98.4% for the pellet containing 9 wt.% LWO.

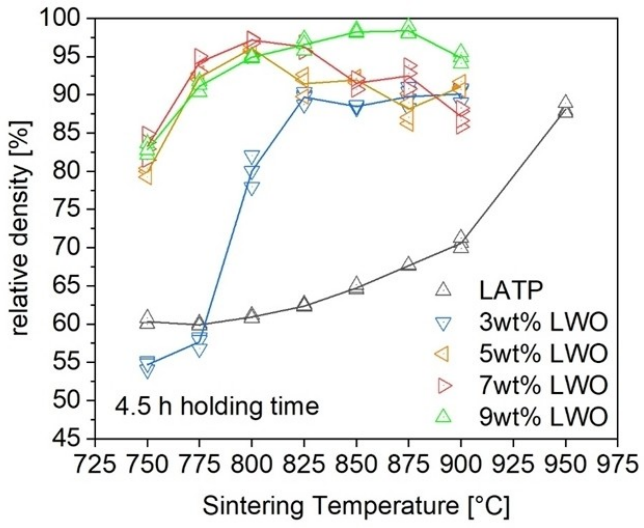

Figure 3. Change of the relative densities with the sintering temperature for varying amounts of Li_2WO_4 (LWO) additive.

The relative density for the samples containing 5–7 wt.% LWO starts to decrease slightly at higher sintering temperatures. For 9 wt.% the decrease was only observed for 900 °C. This behavior is likely attributed to excessive grain growth along with formation of micro-cracks during cooling[8a] due to the high anisotropy of the thermal expansion coefficient.[16] This effect is strongest for the largest grain size and, consequently, the highest sintering temperature.

The relative densities described above agree well with the microstructure of the pellets analyzed by scanning electron microscopy (SEM). Thus, for 5 wt.% LWO with 80% relative density (750 °C, 4.5 h, Figure 4a), the SEM images reveal incomplete sintering with sintering neck formation between the powder particles. The average pore size is about 0.74 μm (max. 3.5 μm).

The 5 wt.% LWO pellet sintered at 800 °C to 96% relative density (Figure 4b) shows a very dense microstructure with few isolated pores with an average size of 0.59 μm, which are apparently responsible for the remaining 5% porosity.

However, the SEM analysis also identifies the presence of isolated particles with the brighter light grey contrast (Figure 4b, marked with red circles). In a separate analysis with backscattered electrons detector (BSE, not shown in Figure 4b), these particles appeared with brighter contrast in comparison to the matrix. As in BSE imaging a higher average atomic number results in brighter contrast, these particles are likely enriched with tungsten. This was confirmed by energy dispersive X-ray spectroscopy (EDX) (Figure 4d inset).

Similar particles with a brighter contrast than the LATP phase are observed for the sample sintered at 825 °C However, here, there are two different types of second phase particles which are clearly different in contrast and, likely, different in W concentration (Figure 4c, blue and red circles).

For the sample sintered at 900 °C (Figure 4d, 6b), which has a lower relative density (91%) as compared to the pellet sintered at 800 °C, the second phase particles change their morphology. Instead of isolated particles, a partially continuous network is formed along the grain boundaries. The grain size increases significantly to 10 μm.

The EDX analysis of these bright areas (Figure 4d, inset) indicates a high local W concentration, while the bulk phase matches well with LATP (Ti, Al, P, and O). The strong growth of the LATP crystals at 900 °C is accompanied by the formation of micro-cracks (Figure 4d), which is typically attributed to the anisotropy in thermal expansion of the LATP crystal structure.[5a,d]

The X-ray diffraction (XRD) analysis (Figure 5) of the pellets containing 9 wt.% LWO indicates a NaSICON structure of LATP (ICSD PDF2: 00 024 0660:7930) as the major phase after sintering at 900 °C . For the LATP without any LWO, small amounts of $LiTiPO_5$ (ICSD PDF2: 00-044-0083) and $Al(PO_4)$ (ICSD PDF2: 01-072-7638) as impurities were detected for both the

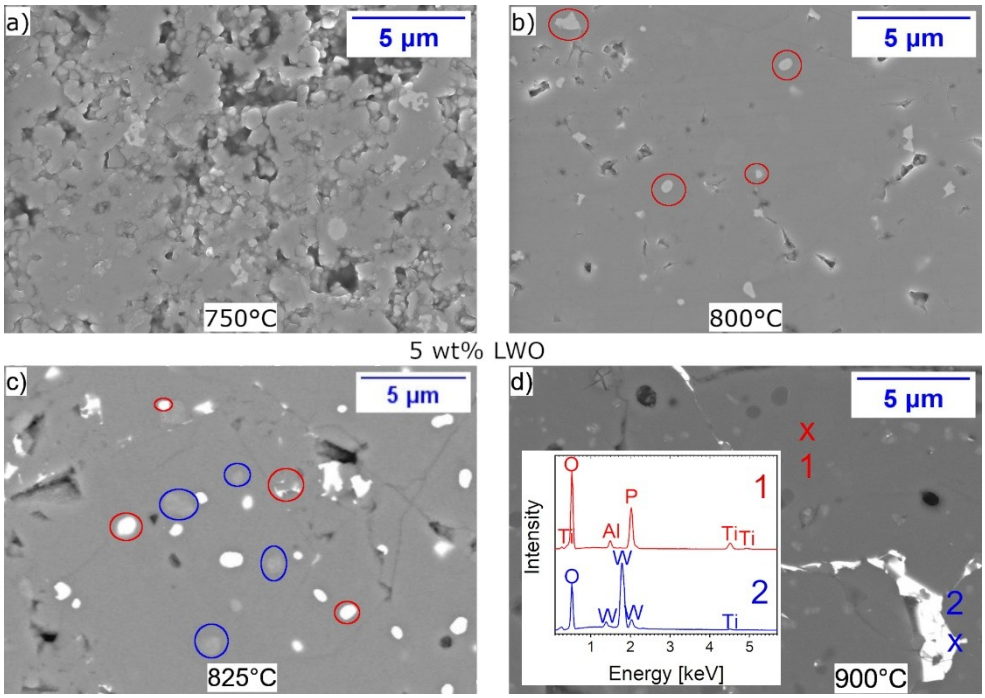

Figure 4. SEM images (with BSE) detector) of LATP – 5 wt.% LWO pellets sintered at: a) 750 °C, b) 800 °C, with the red circles labelling the W-enriched particles with the brighter light grey contrast, c) 825 °C with the red and blue circles labelling the two W-enriched phases, and d) 900 °C. An inset in Figure 4d shows EDX results of an LATP grain (1) and a white area at the grain boundary (2). Ti lines detected in the white domains (point 2) are attributed to the emission of Ti atoms from neighboring LATP grains due to a large excitation volume of several μm^3 ranging into neighboring areas.

powder and the pellets sintered at temperatures of up to 950 °C. After sintering the LWO-containing pellets at 900 °C, $Al(PO_4)$ is no longer detectable, but an additional phase appears in the diffractogram whose relative amount increases with the increasing concentration of LWO in the initial mixture. Surprisingly, this new phase does not correspond to LWO, but was identified as WO_3 (ICSD PDF2: 01-075-2072 : 31823).

Combining the results of XRD, SEM and EDX analysis, the dark grey areas in the SEM images showing the presence of Ti, Al and P can be assigned to LATP. The white areas observed in the SEM images can be assigned to the WO_3, while the light grey areas could correspond to a low amount of a Li-W-O phase that is below the sensitivity limit of the XRD analysis (W containing phase like some Li-enriched tungsten oxide phase). The presence of WO_3 (melting at 1473 °C) indicates that the Li ions of LWO diffused into the LATP structure and were integrated into the material during sintering. It is also possible that some amount of Li evaporates from the liquid LWO phase after melting.

As the melting temperature of LWO is reported as 742 °C,[14] it can be suggested that the sintering of LATP powder in the presence of LWO takes place via a liquid phase mechanism.

A detailed discussion of liquid phase sintering is given by Wang et al.[17] who have demonstrated that the mass transport of lithium through the liquid phase by a solution-precipitation mechanism supports the sintering process. Another process supporting densification is the redistribution of the liquid by capillary stresses and solution precipitation.

Figure 6b shows the microstructure of the W-rich second phase pockets after sintering. Analogous to the small second phase particles in Figure 4c, the presence of two different W-rich phases is observed (as there are bright pockets with two distinctly different brightness), with one of them being identified as WO_3. Beyond the two W-rich second phases, lamellae of LATP were formed in the pockets.

The microstructure and phase composition of the second phase points to a mechanism where liquid LWO is formed initially. As the temperature is increased during sintering, parts of the main phase LATP are dissolved in the melt. During cooling parts of the liquid phase solidify, likely by eutectic solidification.[17] This leads to the formation of lamellae and particles within the molten tungstate, resulting in the structure shown in Figure 6b, and leaving pockets of melt. As the temperature decreases further, the remaining liquid solidifies as well leading to solid WO_3 and an unknown solid phase. The suggestion of a liquid phase sintering mechanism in the presence of LWO is supported by the formation of melt films wetting the grain boundaries as visible in the SEM images along a grain boundary (Figure 6b, green circle and Figure 4d). Likely, the reaction of the molten LWO and the formation of an eutectic melt result in the second shoulder of the densification curves observed in Figure 2.

In the sintering temperature range between 825 °C and 900 °C the morphology of the second phase changes. At 825 °C, no lamellae could be observed. At 900 °C the pellet containing 5 wt.% LWO showed large areas of W-rich melt (mean diameter 2.3 µm; max 22.3 µm) containing large (0.9 µm) LATP lamellae

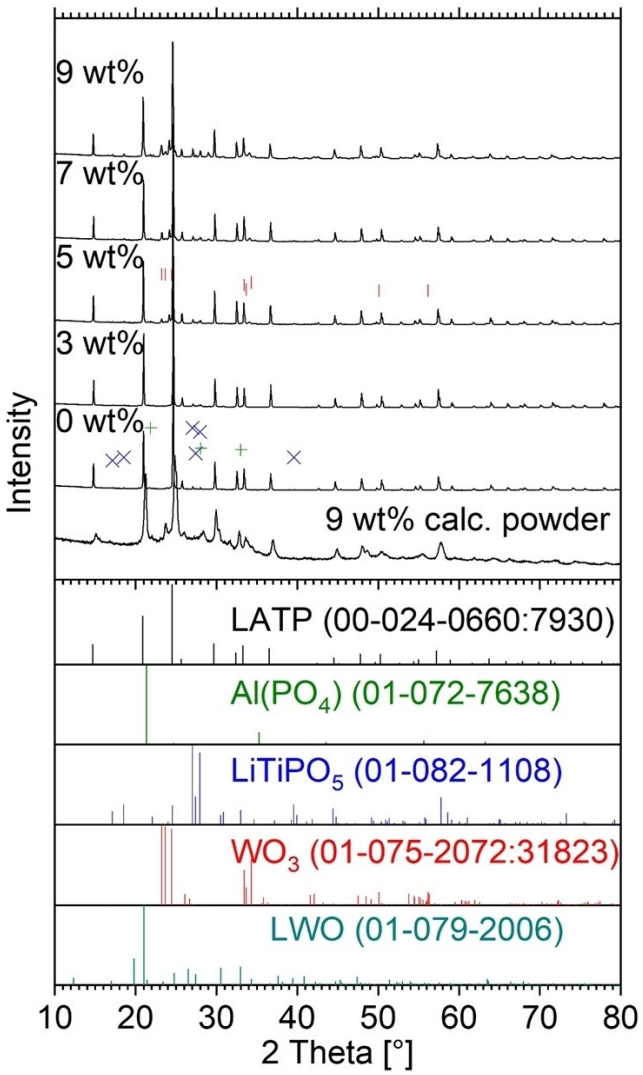

Figure 5. X-ray diffraction patterns of LATP-LWO pellets sintered at 900 °C with different amounts of LWO as indicated. XRD pattern labelled as 9 wt.% powder not sintered refers to the calcined powder.

as well as some small LATP grains (0.5 μm) (Figure 6b), which are very different from the morphology of LATP sintered at the same temperature without LWO addition (Figure 6a). The lamellae point to eutectic solidification. The small LATP grains, which show the facetted features of rhombohedral structure, are likely seeds formed in the melt. These observations indicate that the chemical reaction and subsequent decomposition of the liquid second phase occurs between 825 °C and 900 °C.

Note that this temperature range agrees with the second shoulder of the densification curves in Figure 2. Likely the increase in molten W-rich phases at lower sintering temperatures leads to the ability of grain rearrangement by liquid phase transport, resulting in higher densities. At the same time, a competing process is grain growth in general resulting in very large grain sizes and crack formation, which is a common phenomenon observed in LATP, and reduces the density.[5d]

Ionic conductivity as a function of sintering temperature for different LWO concentrations has been determined using electrochemical impedance spectroscopy (EIS, Figure 7). The spectra were recorded in the frequency range from 7 MHz to 1 Hz. In general, the Nyquist plots (Figure 7 insets) of the sintered LATP-LWO pellets show one semi-circle at high frequencies, corresponding to the transport across the grain boundaries (10^{-11} to 10^{-8} F)[18] and a straight line at medium and low frequencies, associated with the capacitive charging of the electrodes. For the fitting of the impedance plots a "brick-wall" model discussed by Irvine et al. was used,[18] which describes polycrystalline ceramics as three-dimensionally arranged cuboid particles (bricks) separated by grain boundaries. This is an acceptable simplification for more complex grain shapes and can be somewhat mitigated by the use of a non-ideal capacitor, i.e., a constant phase element.[18] An equivalent circuit model was used to fit the data (Figure 7a–e) consisting of constant phase element CPE1 (representing the blocking electrodes) in series with a parallel circuit of R2 and a constant phase element CPE2 (representing the grain boundary resistance) and a bulk grain resistance R1. The bulk grain impedance can be generally resolved as a second semicircle at lower temperatures, however only the real part of the grain impedance (R1) can be observed at room temperature. The sum of R1 and R2 corresponds to the total resistance R_{tot} composed of the bulk and the grain boundary resistance. The total ionic conductivity is then calculated by the ratio of thickness of the sample d and product of the total resistance and the area A of the sample $\sigma_{tot} = d/(R_{tot} \times A)$.For every additive concentration the processing parameters and the corresponding highest ionic conductivity is listed in Table 2 as example. The data includes

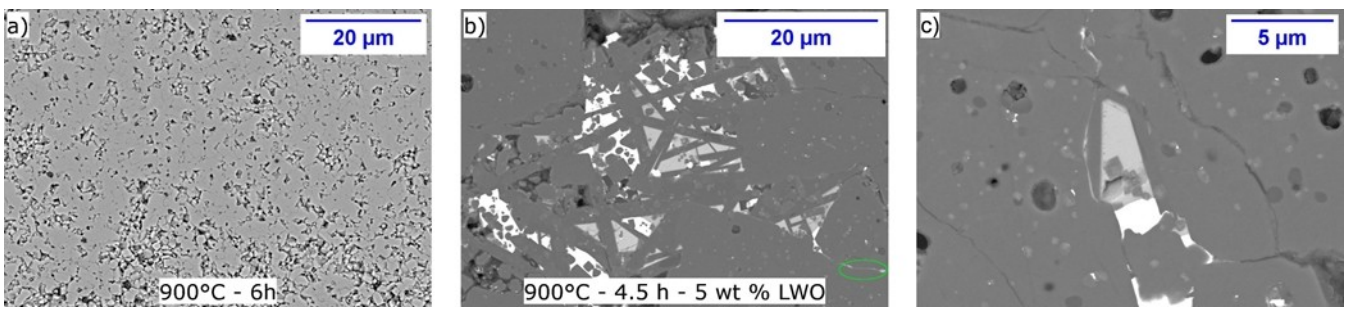

Figure 6. SEM images of the samples sintered at 900 °C: a) pure LATP [BSE] and b and c) LATP with 5 wt% LWO additive [BSE] (green circle: wetting of grain boundary).

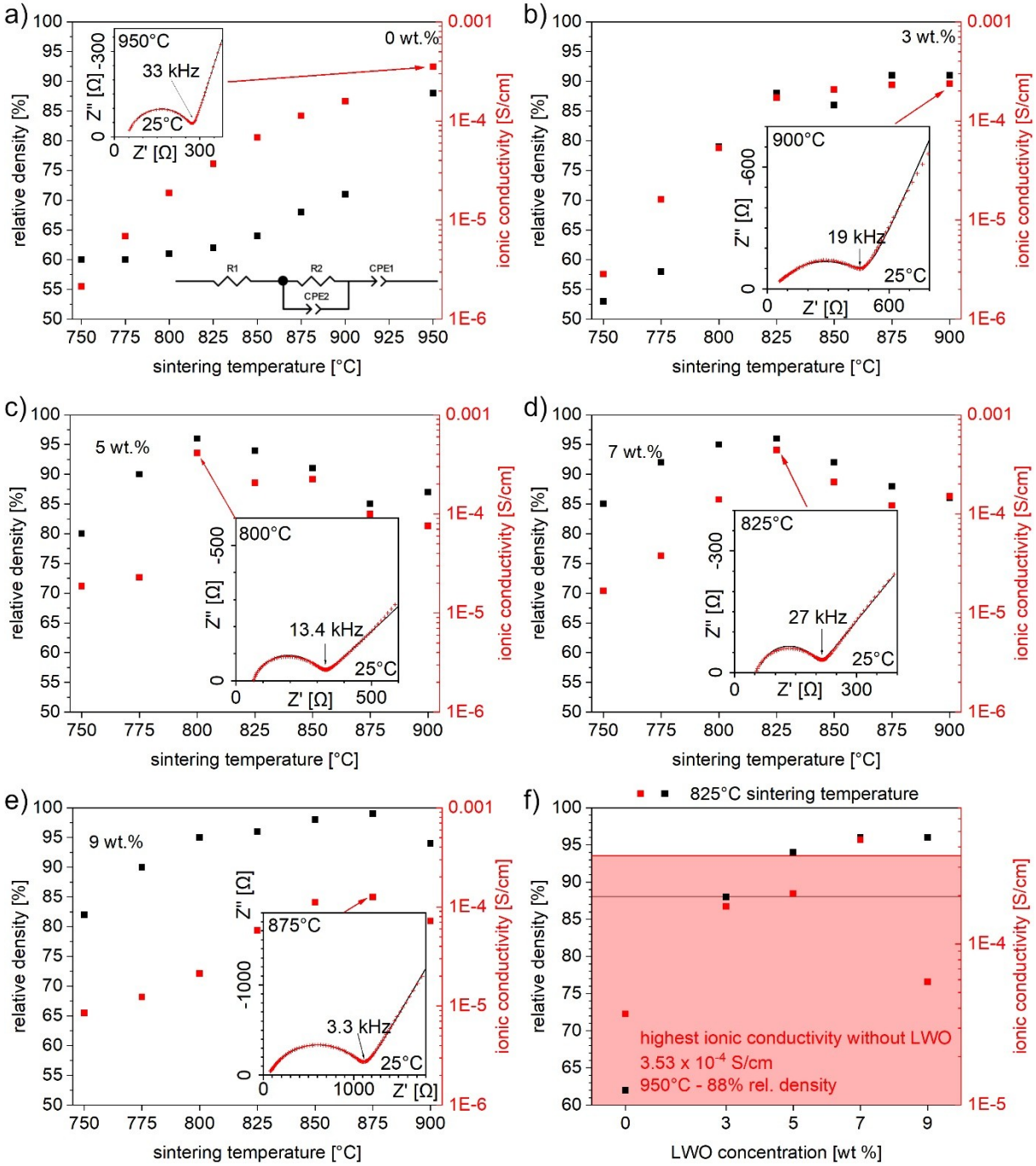

Figure 7. Ionic conductivity and relative density in relation to the sintering temperature of LATP pellets containing a) 0 wt.% b) 3 wt.%, c) 5 wt.%, d) 7 wt.% and e) 9 wt.% LWO. Insets show the impedance spectrum and the fitting curve for the most conductive sample and the equivalent circuit used). f) Ionic conductivity and relative density related to LWO concentration at 825 °C and lines showing the maximum values achieved for the sample without LWO sintered at 950 °C (Note: conductivity in all diagrams is plotted in logarithmic scale).

also the measured values used for the calculation of the total ionic conductivity.

Figure 7 portrays the total ionic conductivity derived from the resistance values for the different LWO contents in relation to the sintering temperature. For all samples, the ionic conductivity increases significantly with the sintering temperature (up to an optimum temperature value discussed above) and is proportional to the increase in the relative density.

The ionic conductivity of LWO-containing pellets is generally higher than that of pure LATP sintered at the same temperature. For the sintering temperature of 825 °C, at which pure LATP does not sinter and shows a very low ionic conductivity of 3.7×10^{-5} S/cm, the pellets containing 3 to 7 wt.% LWO show high ionic conductivity of 1.7×10^{-4}–4.4×10^{-4} S/cm. However, for the sample containing 9 wt.% LWO the ionic conductivity is rather low (5.8×10^{-5} S/cm) in spite of a

Table 2. Fitting parameters R2 and CPE2 (CPE-T: Amplitude; CPE-P: degree of deviation from ideal case) in relation to the LWO concentration and the sintering temperature.

LWO [wt%]	Temperature [°C]	R1 [Ω]	R2 [Ω]	CPE2-T	CPE2-P	σ_{tot} [mS/cm]
	950	56	203	5.72×10^{-9}	0.93	0.35
3	900	45	435	1.65×10^{-7}	0.67	0.24
5	800	64	242	2.58×10^{-8}	0.81	0.41
7	825	59	138	8.53×10^{-9}	0.93	0.44
9	875	57	1059	7.12×10^{-8}	0.71	0.13

high relative density (98.4%) (Figure 7f). A possible explanation for the lower values is the presence of highly resistive grain boundaries due to a wetting layer of WO_3 as observed in the SEM images.

The highest total ionic conductivities were obtained for the samples with the additive concentration of 5 wt.% sintered at 800 °C, reaching a value of 4.1×10^{-4} S/cm, and for the 7 wt.% LWO sintered at 825 °C reaching the conductivity of 4.4×10^{-4} S/cm, both with relative densities of 96%. The conductivity of the samples containing 7 wt.% and sintered at 825 °C (4.4×10^{-4} S/cm) is higher than the value 3.5×10^{-4} S/cm (88%), which however was achieved for the reference pellets sintered at a much higher sintering temperature of 950 °C. The sintering temperature was decreased by 150 K compared to pure LATP.

This study shows the effect of two competing factors on the ionic conductivity: The relative density and resistive WO_3 films. The relative densities can be significantly improved with the addition of LWO. A viable density (>90%) is reached at a lowered sintering temperature of 775 °C for 5, 7 and 9 wt.% LWO. The highest relative density is reached for 9 wt.% LWO sintered at 875 °C, but the ionic conductivity for this sample was recorded with 1.3×10^{-4} S/cm. The whole data set for 9 wt.% shows low ionic conductivities, while the relative densities are high. Therefore, there is a competing factor that hinders ionic conduction in these highly dense samples. WO_3 films were identified at the grain boundaries by XRD and SEM and it is argued that these layers are introducing additional resistance in the samples. As the amount of WO_3 at the grain boundaries increases with a higher LWO addition it can be argued that with 7 wt.% a threshold is reached. For higher additive concentrations the contribution from the resistive films begins to dominate.

It should be mentioned that the quality of LATP powder critically depends on the synthesis and processing conditions and that the batch of LATP powder used in this work did not reach the highest conductivity mainly due to the presence of $LiTiPO_5$ impurities in the microstructure, which were present after sintering for all of the samples. It can therefore be expected that even higher conductivity values may be obtained with the LWO sintering aid for LATP powders with higher phase purity and optimized powder morphology.

Table 3 gives an overview of conductivity values reported in the literature achieved for different LATP materials with different sintering aids together with the values obtained in this work. The comparison of conductivity values for different polycrystalline materials is generally difficult, as the total conductivity depends on the bulk ionic conductivity (upper conductivity limit) of LATP phase as well as the grain size distribution and shape, which differ for different materials and whose impact cannot be compared systematically. In general, Table 3 shows that the sintering temperature is significantly decreased to temperatures as low as 800 °C with the addition of LWO and the ionic conductivity for such a low sintering temperature is exceeding many results from other studies. The table contains a few examples with higher conductivity values: (i) GeO_2,[21] which was, however, sintered at a much higher temperature (950 °C). The cost of Ge is an aspect that renders the use of GeO_2 very improbable; (ii) Bi_2O_3[13] was used in

Table 3. Ionic conductivity of published LATP ceramic materials with the used sintering aid, the recorded sintering conditions, density and obtained ionic conductivities.

LATP composition	Sintering aid	Ionic conductivity S/cm	Sintering conditions	Density %	Ref.
$Li_{1.3}Al_{0.3}Ti_{1.7}(PO_4)_3$	–	3.8×10^{-4}	1080 °C, 1 h	89.8	[9b]
$Li_{1.3}Al_{0.3}Ti_{1.7}(PO_4)_3$	Li_3BO_3 (15 mol%)	9.8×10^{-5}	740 °C, 1 h	92.4	[9b]
$Li_{1.3}Al_{0.3}Ti_{1.7}(PO_4)_3$	Li_3PO_4 (15 mol%)	2.9×10^{-4}	820 °C, 1 h	92.7	[9b]
$Li_{1.3}Al_{0.3}Ti_{1.7}(PO_4)_3$	Li_2CO_3 (15 mol%)	3.8×10^{-4}	840 °C, 1 h	95.5	[9b]
$Li_{1.5}Al_{0.5}Ti_{1.5}(PO_4)_3$	–	2.9×10^{-4}	900 °C, 5 h	92.5	[2b]
$Li_{1.5}Al_{0.5}Ti_{1.5}(PO_4)_3$	$Li_2B_4O_7$ (0.5 wt.%)	5.8×10^{-4}	900 °C, 5 h	92	[2b]
$Li_{1.5}Al_{0.5}Ti_{1.5}(PO_4)_3$	–	6.9×10^{-4}	880 °C, 5 h	95	[19]
$Li_{1.3}Al_{0.3}Ti_{1.7}(PO_4)_3$	–	7×10^{-4}	980–1000 °C, 2 h	95.9	[3]
$Li_{1.4}Al_{0.4}Ge_{0.2}Ti_{1.4}(PO_4)_3$	–	$1{,}2\times10^{-3}$	900 °C, 14 h	95.3	[20]
$Li_{1.4}Al_{0.4}Ti_{1.6}(PO_4)_3$	GeO_2 (3 wt.%)	1.15×10^{-3}	950 °C, 7 h	93.3	[21]
$Li_{1.3}Al_{0.3}Ti_{1.7}(PO_4)_3$	$LiBO_2$ (1 wt.%)	3.5×10^{-4}	800 °C, 2 h	97.1	[10]
$Li_{1.3}Al_{0.3}Ti_{1.7}(PO_4)_3$	$LiBF_4$ (3 wt.%)	8.5×10^{-4}	800 °C, 6 h	98.2	[12]
$Li_{1.4}Al_{0.4}Ti_{1.6}(PO_4)_3$	–	1.83×10^{-4}	900 °C, 6 h	97	[22]
$Li_{1.5}Al_{0.5}Ge_{1.5}(PO_4)_3$	B_2O_3 (0.05 wt.%)	6.9×10^{-4}	825 °C, 5 h (recryst.)		[23]
$Li_{1.3}Al_{0.3}Ti_{1.7}(PO_4)_3$	LiF (0.1 n)	1.1×10^{-4}	800 °C	94.2	[11]
$Li_{1.4}Al_{0.4}Ti_{1.6}(PO_4)_3$	Bi_2O_3 (1 wt.%)	9.4×10^{-4}	850 °C		[13]
$Li_{1.3}Al_{0.3}Ti_{1.7}(PO_4)_3$	WO_3 (5 wt.%)	5.49×10^{-4}	950 °C, 4 h		[24]
$Li_{1.3}Al_{0.3}Ti_{1.7}(PO_4)_3$	–	1.15×10^{-4}	950 °C, 12 h (recryst.)		[25]
$Li_{1.5}Al_{0.5}Ti_{1.5}(PO_4)_3$	–	3.5×10^{-4}	950 °C, 4.5 h	88	This work
$Li_{1.5}Al_{0.5}Ti_{1.5}(PO_4)_3$	Li_2WO_4 (5 wt.%)	4.1×10^{-4}	800 °C, 4.5 h	96	This work
$Li_{1.5}Al_{0.5}Ti_{1.5}(PO_4)_3$	Li_2WO_4 (7 wt.%)	4.4×10^{-4}	825 °C, 4.5 h	96	This work

combination with 25 K higher sintering temperatures (850 °C); $LiBF_4$[12] delivered high ionic conductivity at the same sintering temperature, however, the composition of the original LATP powder was different to the LATP material used in this work.

Overall, the sintering aid LWO offers the potential of reduced sintering temperatures while maintaining the high conductivity of LATP. For the processing of solid-state batteries, this decrease in sintering temperature might limit the decomposition of cathode active materials and the amount of chemical reactions at the interface between cathode and electrolyte.

Conclusion

An approach to lower the sintering temperature of LATP is the use of a sintering aid. In this work LWO was used for the first time as a sintering aid for the densification of $Li_{1.5}Al_{0.5}Ti_{1.5}(PO_4)_3$. It enables sintering the material at 800 °C to sufficiently high density while at the same time maintaining the high total ionic conductivity. With the addition of LWO the microstructure was improved even for temperatures as low as 800 °C showing less pores leading to a better contact between the grains. This coincided with an increase in relative density from 61 % for the LATP sample to 96 % for LATP mixed with 5 wt.% of LWO. Even higher relative densities for samples with 9 wt.% LWO lead to significantly reduced ionic conduction due to the formation of highly resistive WO_3 films at the grain boundaries. The relative densities decreased when the sintering temperatures exceeded 825 °C due to excessive grain growth and microcrack formation. An addition of 7 wt% of LWO was most successful for the densification (96 %, 825 °C) as well as for the conductivity (4.4×10^{-4} S/cm). Significant reduction in sintering temperature and at the same time increase in the ionic conductivity of LATP achieved with only a small weight fraction of LWO render LWO a very promising sintering aid for the development of LATP-based solid-state batteries.

Experimental Section

The synthesis of $Li_{1.5}Al_{0.5}Ti_{1.5}(PO_4)_3$ is based on a solution-assisted solid-state reaction (SASSR) as described elsewhere.[2b] Typically, a stoichiometric amount (211.13 g) of lithium dihydrogen phosphate LiH_2PO_4 (97 %, Alfa Aesar, A16987) was dissolved under continuous stirring in water (3 L) at room temperature followed by the addition of an aqueous solution of aluminum acetate (816.72 g, Alfa Aesar A11620). The Al content was determined via gravimetric analysis resulting in a concentration of 4.1 wt.% based on two measurements. Afterwards, 133 ml of phosphoric acid H_3PO_4 (85 %, BASF, 50488884) was added resulting in a mixture with a pH value of 2. In the final step, 571.49 g of titanium(IV) isopropoxide $Ti[OCH(CH_3)_2]_4$ (97 %, Acros, 194700010) was added resulting in a white precipitate. The suspension was stirred for 4 h at room temperature. The temperature was monitored and kept below 40 °C. The reaction mixture was dried at 80 °C for 48 h. The retained solid white agglomerates were placed in an Al_2O_3 crucible and heated to 600 °C for 5 h with a heating and cooling rate of 180 K/h. After calcination, the powder was crushed in a mortar and further milled by a planetary ball mill (Fritsch Pulverisette 7, 500 rpm) for 3 h using 10 mm zirconia balls. After milling, the mixture including the balls was put in a bottle with ethanol and placed on a roller bench for 12 h. Li_2WO_4 (99 %, Alfa Aesar, 43366) was milled in the same manner. The milled and dried LATP was combined with 3, 5, 7, and 9 wt.% of milled Li_2WO_4 (LWO), dispersed in ethanol, and mixed on the roller bench using 10 mm zirconia balls (12 h). Subsequently, the powder mixture was dried and sieved (100 μm).

The stoichiometry of the powders and crushed sintered pellets was determined by inductively coupled plasma optical emission spectroscopy (ICP-OES). The powders were characterized by laser diffraction (Horiba LA 950 V2) to gain information on the particle size distribution. The measurement was conducted in ethanol and the suspension was ultrasonicated to break up agglomerates. X-ray diffraction (XRD) patterns were recorded using a Bruker D4 X ray diffractometer.

The powders, mixed with a few drops of glycerine to facilitate the pressing procedure (4 drops/1 g), were pressed to pellets in a 13 mm die at a pressure of 75 MPa. The relative geometric green density was 55 %. The samples were sintered in Al_2O_3 crucibles in a muffle furnace at temperatures between 750 °C and 900 °C for 4.5 hours. The heating rate was 60 K/h to 500 °C and 300 K/h to the sintering temperature. The cooling rate was 60 K/h. The height, diameter and weight of the pellets were recorded to calculate their density. To evaluate the sintering behavior, the dilatometric shrinkage was determined for pressed pellets without glycerine having a diameter of 8 mm and height of 1.8 mm (DIL 402 C, Netzsch). A constant heating rate of 300 K/h was applied to a final temperature of 1100 °C.

Cross-sections were prepared for scanning electron microscopy (SEM) by embedding the samples in EpoFix® resin and subsequent grinding and polishing with water free media. The samples were sputter-coated with platinum. SEM images were acquired with a Zeiss Ultra 55 SEM scanning electron microscope at 8 kV. Energy-dispersive X ray (EDX) analysis was conducted at an operating voltage of 10 kV using a X–Max EDX detector with 80 mm^2 detector area (Oxford Instruments) and Inca acquisition software.

For conductivity measurements, the surface of the pellets was polished with grinding paper (starting at 800 up to 4000) followed by the application of gold electrodes (blocking electrodes) by sputtering. These samples were fixed in EL cells® in an Ar filled glovebox. Impedance spectra were recorded at room temperature in the range from 7 MHz to 1 Hz (VMP 300; Biologic SAS) and fitted with Z view software (Scribner Associates Inc.).

Acknowledgements

The authors thank Dr. D. Sebold for SEM investigations, M. T. Gerhards for dilatometry measurements, and Dr. Y. J. Sohn for the HT-XRD analysis. The authors would also like to acknowledge the financial support by the German Federal Ministry of Education and Research in the Kompetenzcluster für Festkörperbatterien FESTBATT (13XP0173A) and CatSE Project (13XP0223A). W. R. acknowledges funding by the DFG (RH 146/1).The authors take responsibility for the content of this publication. Open Access funding enabled and organized by Projekt DEAL.

Conflict of Interest

The authors declare no conflict of interest.

Keywords: Ceramics · Crystal growth · Lithium-ion conductor NASICON-type · Solid electrolyte

[1] a) A. Manthiram, X. W. Yu, S. F. Wang, *Nat. Rev. Mater.* **2017**, *2*, 16; b) S. Randau, D. A. Weber, O. Kotz, R. Koerver, P. Braun, A. Weber, E. Ivers-Tiffee, T. Adermann, J. Kulisch, W. G. Zeier, F. H. Richter, J. Janek, *Nat. Energy* **2020**, *5*, 259–270; c) M. S. Whittingham, *J. Power Sources* **2020**, *473*, 228574.
[2] a) Z. Z. Zhang, Y. J. Shao, B. Lotsch, Y. S. Hu, H. Li, J. Janek, L. F. Nazar, C. W. Nan, J. Maier, M. Armand, L. Q. Chen, *Energy Environ. Sci.* **2018**, *11*, 1945–1976; b) B. Davaasuren, F. Tietz, *Solid State Ionics* **2019**, *338*, 144–152.
[3] H. Aono, E. Sugimoto, Y. Sadaoka, N. Imanaka, G. Adachi, *J. Electrochem. Soc.* **1990**, *137*, 1023–1027.
[4] a) A. Sano, Google Patents, **2008**; b) M. Yoshioka, M. Ouchi, T. Hayashi, K. Nishida, Google Patents, **2013**.
[5] a) S. D. Jackman, R. A. Cutler, *J. Power Sources* **2012**, *218*, 65–72; b) E. C. Bucharsky, K. G. Schell, A. Hintennach, M. J. Hoffmann, *Solid State Ionics* **2015**, *274*, 77–82; c) G. J. Redhammer, D. Rettenwander, S. Pristat, E. Dashjav, C. M. N. Kumar, D. Topa, F. Tietz, *Solid State Sci.* **2016**, *60*, 99–107; d) K. Waetzig, A. Rost, U. Langklotz, B. Matthey, J. Schilm, *J. Eur. Ceram. Soc.* **2016**, *36*, 1995–2001.
[6] a) L. Miara, A. Windmuller, C. L. Tsai, W. D. Richards, Q. Ma, S. Uhlenbruck, O. Guillon, G. Ceder, *ACS Appl. Mater. Interfaces* **2016**, *8*, 26842–26850; b) M. Gellert, E. Dashjav, D. Gruner, Q. L. Ma, F. Tietz, *Ionics* **2018**, *24*, 1001–1006.
[7] a) P. Y. Xu, W. Rheinheimer, S. N. Shuvo, Z. M. Qi, O. Levit, H. Y. Wang, Y. Ein-Eli, L. A. Stanciu, *ChemElectroChem* **2019**, *6*, 4576–4585; b) P. Y. Xu, W. Rheinheimer, A. Mishra, S. N. Shuvo, Z. M. Qi, H. Y. Wang, A. M. Dongare, L. A. Stanciu, *ChemElectroChem* **2021**, *8*, 1847–1857.
[8] a) M. N. Rahaman, *Ceramic processing and sintering, Vol. 23*, Second edition ed., Taylor & Francis, Boca Raton, FL, **2003**; b) S.-J. L. Kang, *Sintering : densification, grain growth, and microstructure [E-Book]*, Elsevier Butterworth-Heinemann, Amsterdam, **2005**.
[9] a) H. Aono, E. Sugimoto, Y. Sadaoka, N. Imanaka, G. Adachi, *Solid State Ionics* **1991**, *47*, 257–264; b) K. Waetzig, C. Heubner, M. Kusnezoff, *Crystals* **2020**, *10*, 11.
[10] H. Bai, J. Hu, X. Li, Y. Duan, F. Shao, T. Kozawa, M. Naito, J. Zhang, *Ceram. Int.* **2018**, *44*, 6558–6563.
[11] K. Kwatek, W. Slubowska, J. Trebosc, O. Lafon, J. Nowinski, *J. Eur. Ceram. Soc.* **2020**, *40*, 85–93.
[12] L. J. Dai, J. Wang, Z. X. Shi, L. N. Yu, J. Shi, *Ceram. Int.* **2021**, *47*, 11662–11667.
[13] S. D. Lee, K. N. Jung, H. Kim, H. S. Shin, S. W. Song, M. S. Park, J. W. Lee, *ChemSusChem* **2017**, *10*, 2175–2181.
[14] L. L. Y. Chang, S. Sachdev, *J. Am. Ceram. Soc.* **1975**, *58*, 267–270.
[15] P. Tabero, A. Frackowiak, *J. Therm. Anal. Calorim.* **2017**, *130*, 311–318.
[16] T. Hupfer, E. C. Bucharsky, K. G. Schell, A. Senyshyn, M. Monchak, M. J. Hoffmann, H. Ehrenberg, *Solid State Ionics* **2016**, *288*, 235–239.
[17] Z. Wang, L. Song, J. J. Bian, *Ceram. Int.* **2013**, *39*, 9767–9772.
[18] J. T. S. Irvine, D. C. Sinclair, A. R. West, *Adv. Mater.* **1990**, *2*, 132–138.
[19] Q. L. Ma, Q. Xu, C. L. Tsai, F. Tietz, O. Guillon, *J. Am. Ceram. Soc.* **2016**, *99*, 410–414.
[20] F. Bai, K. Kakimoto, X. F. Shang, D. Mori, S. Taminato, M. Matsumoto, Y. Takeda, O. Yamamoto, H. Minami, H. Izumi, N. Imanishi, *J. Asian Ceram. Soc.* **2020**, *8*, 476–483.
[21] F. Bai, X. F. Shang, H. Nemori, M. Nomura, D. Mori, M. Matsumoto, N. Kyono, Y. Takeda, O. Yamamoto, N. Imanishi, *Solid State Ionics* **2019**, *329*, 40–45.
[22] L. Z. Huang, Z. Y. Wen, M. F. Wu, X. W. Wu, Y. Liu, X. Y. Wang, *J. Power Sources* **2011**, *196*, 6943–6946.
[23] H. S. Jadhav, M. S. Cho, R. S. Kalubarme, J. S. Lee, K. N. Jung, K. H. Shin, C. J. Park, *J. Power Sources* **2013**, *241*, 502–508.
[24] X. J. Lu, F. L. Meng, S. Huang, D. Zhao, *Mater. Lett.* **2018**, *230*, 177–179.
[25] J. S. Thokchom, B. Kumar, *Solid State Ionics* **2006**, *177*, 727–732.

Manuscript received: October 8, 2021
Revised manuscript received: November 10, 2021
Accepted manuscript online: November 17, 2021